A Cascaded Learning Framework for Road Profile Estimation Using Multiple Heterogeneous Vehicles

Zhu Chen

Department of Mechanical and Aerospace Engineering, University at Buffalo,

Buffalo, NY 14260

e-mail: zhuchen@buffalo.edu

Mohammad R. Hajidavalloo

Department of Mechanical Engineering, Michigan State University, East Lansing, MI 48824 e-mail: hajidava@msu.edu

Zhaojian Li

Department of Mechanical Engineering, Michigan State University, East Lansing, MI 48824 e-mail: lizhaoj1@egr.msu.edu

Minghui Zheng¹

Department of Mechanical and Aerospace Engineering, University at Buffalo, Buffalo, NY 14260

e-mail: mhzheng@buffalo.edu

Road profile information can be utilized to enhance vehicle control performance, passenger ride comfort, and route planning and optimization. Existing road-profile estimation algorithms are mainly based on one single vehicle, which are usually susceptible to modeling uncertainties and measurement noises. This technical brief proposes a new cascaded learning framework that utilizes multiple heterogeneous vehicles to achieve enhanced estimation. In this framework, each individual vehicle first performs a local estimation via a standard disturbance observer (DOB) while traversing a considered road segment. Then learning filters are designed to dynamically connect the vehicles, and the preliminary estimates from one vehicle are utilized to generate the learning signal for another. For each vehicle, a heterogeneous learning signal is produced and added to its estimation loop for estimating enhancement, through which the estimations are improved over multiple iterations. Extensive numerical studies are carried out to validate the effectiveness of the proposed method with promising results demonstrated. [DOI: 10.1115/1.4055041]

Introduction

Road profile is an important road feature that affects road vehicles' performance concerning passenger comfort and safety. Road profile information has been frequently used in intelligent automotive systems such as suspension control [1] and comfort-based route planning [2]. Road profile in early days was mainly measured using contact-based profile analyzer (e.g., Refs. [3] and [4]) in which a specially equipped trailer was designed to contact the road surface and provide profile measurements. Noncontact measurements such as laser sensors [5,6] have also been

developed later. Those specially designed road profilers are generally expensive to build and maintain, and thus the measuring coverage is limited. Recently, with built-in accelerometers, gyroscopes, and global position system, smartphones have also been used in road profile estimation due to its wide availability and low cost [7,8]. However, insufficient accuracy is a major setback with smartphone-based methods.

Meanwhile, modern automobiles are equipped with a variety of sensors and communication modules, and can therefore be employed as mobile sensors to crowdsource enormous road profile data sets [9,10]. As a result, vehicle response-based estimating methodologies have been widely studied in order to recover road profile by leveraging on-board sensors as well as the underlying vehicle-road interaction dynamics [11-16]. Most vehicle response-based estimating methods employ a single vehicle for the road profile estimation by leveraging quarter-car model (e.g., Ref. [14]), half-car model (e.g., Ref. [7]), or full car model (e.g., Ref. [15]). To handle the perturbation and uncertainties during the estimation, advanced methods including supertwisting algorithm (STA) (e.g., Ref. [11]), adaptive control and sliding mode controlbased estimation have been proposed (e.g., Refs. [17] and [18]). However, STA is limited to systems with relative degree one, and those mentioned methods usually require the bounds of the input disturbance, which is not always accessible. Besides, those advanced methods are generally used in the disturbance observer (DOB)-based control framework by leveraging the feedback control theory, which requires expertise knowledge. On the other hand, to reduce the dependency of the dynamic model information, data-driven methods such as neural network-based methods (e.g., Refs. [19-21]) have been designed for road profile estimation.

Another line of work is to use multiple estimation iterations or multiple vehicles/systems to improve the estimation robustness (e.g., Refs. [22–24], a collaborative estimation with networked and connected vehicles is studied with a privacy-preservation mechanism, and this study preliminary showed that the estimation with multiple vehicles outperforms that with a single vehicle in terms of the estimation error. In Knowledge transfer has been studied for performance enhancement but applications are limited in areas such as controller design (e.g., Refs. [25] and [26]). Iterative learning identification (e.g., Ref. [27]) has been used for unknown parameter identification. However, iterative learning identification aims to have an optimal estimation of the dynamic model using multiple iterations instead of estimating the input disturbance.

In general, single-vehicle-based estimation highly relies on an accurate model, measurements, and sophisticated algorithms, and the estimation results are thus susceptible to uncertainties. As such, using multiple vehicles for a centralized road profile estimation has great potential since it can increase the estimation reliability by including multiple estimation iterations rather than depending on just one. In order to make the estimation less susceptible to uncertainties while reducing the algorithm complexity, this brief utilizes multiple vehicles and a cascaded learning framework for road profile estimation. In the learning framework, multiple vehicles are employed as learning (estimating) agents, and each learning agent equips a standard DOB to perform a basic estimation of the road profile. The estimation from one agent is recorded and utilized by another subsequent agent for estimation improvement, and by repeating this pattern, the estimation performance is iteratively enhanced. The necessary conditions are derived to guarantee suitable convergence of the learning filter. Numerical studies have been carried out to validate the proposed method where sinusoidal and type-C road profiles [15] are tested.

The main contributions of this paper are listed as follows: (1) the cascaded learning framework offers great flexibility of DOB design, that is, a high-performance DOB design is not required, and the estimation using the basic DOB will be improved through learning iterations. (2) The proposed method is easy to implement;

¹Corresponding author.

Contributed by the Dynamic Systems Division of ASME for publication in the JOURNAL OF DYNAMIC SYSTEMS, MEASUREMENT, AND CONTROL. Manuscript received November 17, 2021; final manuscript received July 14, 2022; published online August 3, 2022. Assoc. Editor: Christopher Vermillion.

unlike other advanced designs such as robust DOBs, it is unnecessary to incorporate a sophisticated feedback controller into the estimation scheme. This allows that vehicles with passive suspension systems can be readily employed in this framework. (3) A weight mechanism is designed to control the error convergence rate in the sense of 2-norm. This can serve as a method to have a smooth learning over the learning axis and avoid aggressive learning scenarios.

The remainder of this paper is organized as follows: Sec. 2 describes the road profile estimation basics, and the problem associated with the single vehicle-based estimation is stated. Section 3 presents the cascaded learning framework including the detailed design of the learning signal, learning filters, and DOB parameters. Section 4 shows the numerical studies and results. Finally, Sec. 5 concludes the paper.

Road Profile Estimation Basics

This brief deals with road profile estimation with vehicle response-based method. The estimation scenario is given in Fig. 1, where it shows a road segment of interest, and l-h is the lateral–horizontal plane, and v-h is the vertical–horizontal plane. Suppose the road profile has pitfalls and bumps and the road information in the vertical direction is our interest. We denote this road profile as v(h), and by considering the road distance in the horizontal direction, the vehicle speed, v(h), can be represented by a time-dependent variable w(t), that is w(t) = v(h), where t means the time.

To obtain the road profile information, usually a road vehicle equipped with sensors is used to traverse the road, and an observer-based algorithm is designed to have the estimation. The basic idea of the observer-based estimation is that we treat the road profile w = w(t) as the disturbance input to the vehicle suspension system G_{ν} ; the output of G_{ν} goes to the designed observer \hat{G}_o and outputs an estimate \hat{w} , which approximates w, as shown in Fig. 2. More details about the observer design can be referred to Ref. [14]. An ideal G_o is expected to correctly invert G_v . However, a highly accurate G_o may not be possible in real case due to several reasons: (1) the modeling uncertainties naturally exist in G_{ν} and it is challenging to obtain $G_o = G_v^{-1}$; (2) a noncausal G_v can result in a causal G_o , which might be not suitable in real-time estimation; and (3) a low-pass filter is usually incorporated into G_o in order to filtrate high-frequency noises, which will introduce delay to the system. Therefore, the single vehicle-based estimation is subject to uncertainties and high-frequency signals. Furthermore, the single vehicle-based design usually depends on an accurate model, sophisticated algorithms, and sometimes includes feedback controller design (e.g., in the DOB-based control framework), and these require extensive tuning and design labors.

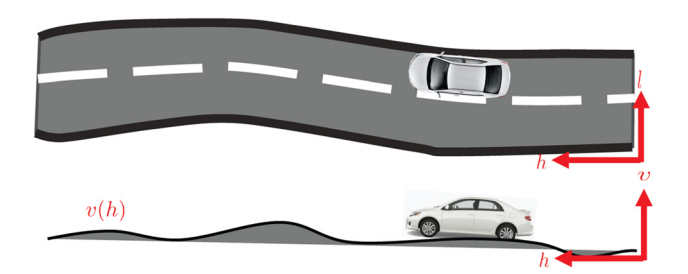


Fig. 1 A road profile to be estimated using a vehicle

$$w G_v(s) \longrightarrow G_o(s) \hat{w}$$

Fig. 2 Observer-based estimation scheme

To make the estimation less easily subject to uncertainties and noises, while reducing the algorithm complexity, this paper proposes a cascaded learning framework which leverages multiple vehicles and basic DOB designs to enhance the estimating performance through a learning mechanism.

Learning-Based Road Profile Estimation

In this section, the cascaded learning framework, which includes multiple vehicles, is first introduced. Then the learning filter and DOB designs are presented, and the learning convergence is demonstrated.

Learning Framework. This subsection presents the proposed learning framework. Specifically, each vehicle is used as an individual estimating (learning) agent by equipping a standard DOB, and the agents are placed on the learning axis. The learning filters dynamically connect two adjacent agents, and the estimation from the previous agent is used to generate a learning signal to enhance the estimation by its adjacent agent.

Denote j as the index of the agent. Consider a specific road segment w (w = v(h)) where multiple agents drive though it for collaborative estimations. The learning framework is shown in Fig. 3, where the variables are defined as follows. For agent j, denote P_j and \hat{P}_j as its actual and nominal models, respectively; D_j is the standard DOB equipped in the agent; $L_{1,j}$ and $L_{2,j}$ denote two learning filters to be designed which are associated with the agent j. Agent P_j drives through the road profile w to have a measurement y_j , and y_j goes through the D_j to generate an estimation \hat{w}_j^o ; the learning filters take the estimation knowledge from agent (j-1) and generate a learning signal \hat{w}_j^f to compensate \hat{w}_j^o ; the compensated estimation \hat{w}_j goes through the nominal model \hat{P}_j to have an output \hat{y}_j ; the difference between y_j and \hat{y}_j is defined as the measurement error e_j , and the difference between w_j and \hat{w}_j is defined as the disturbance estimation error.

To reduce the disturbance estimation error, we first consider reducing the measurement error e_j through the learning iterations. To this end, e_j is first related to e_{j-1} . Since there are two inputs $(\hat{w}_j^f \text{ and } w)$ to the system, we define S_j as the dynamics from the learning signal \hat{w}_j^f to e_j , and denote T_j as the dynamics from w to e_j . For compactness purposes, the frequency domain operator 's' of the transfer functions is omitted in the contexts. For example, S_j represents $S_j(s)$. Then we have

$$S_j = \hat{P}_j$$

$$T_i = P_i D_i \hat{P}_i - P_i$$
(1)

and

$$e_j = S_j \{\hat{w}_i^f\} + T_j \{w\}$$
 (2)

Design the learning signal as

$$\hat{w}_{j}^{f} = k_{j}(L_{1,j}\{\hat{w}_{j-1}^{f}\} + L_{2,j}\{e_{j-1}\})$$
(3)

where

$$k_j = \begin{cases} \eta j \text{ for } 0 < \eta j < 1\\ 1 \text{ for } \eta j \ge 1 \end{cases} \tag{4}$$

and η (0 < η < 1) is a constant scalar. The purpose of k_j is to control the convergence rate of the error e_j , and different forms of k_j will result in different convergence rates. More details regarding this are illustrated in later contexts. From Eq. (2), it follows that

$$\hat{w}_{j-1}^f = S_{j-1}^{-1} \{ e_{j-1} - T_{j-1} \{ w \} \}$$
 (5)

Plugging Eq. (3) into Eq. (2) yields

$$e_j = S_j \{ k_j (L_{1,j} \hat{w}_{j-1}^f + L_{2,j} e_{j-1}) \} + T_j \{ w \}$$
 (6)

and plug Eq. (5) into Eq. (6), we have

$$e_{j} = k_{j}(S_{j}L_{2,j} + S_{j}L_{1,j}S_{j-1}^{-1})\{e_{j-1}\}$$

$$+ (T_{j} - k_{i}S_{i}L_{1,j}S_{j-1}^{-1}T_{j-1})\{w\}$$

$$(7)$$

From now on e_j is related to e_{j-1} . In order to make e_j decrease iteratively, one possible method is to transfer the problem into the following optimization problem:

Step 1:
$$\min_{L_{1,j}} ||T_j - k_j S_j L_{1,j} S_{j-1}^{-1} T_{j-1}||$$

Step 2: $\min_{L_{2,j}} ||k_j (S_j L_{2,j} + S_j L_{1,j} S_{j-1}^{-1})||$ (8)

Equation (8) shows that $L_{1,j}$ and $L_{2,j}$ can be obtained step by step, and the sufficient condition to make $||e_j|| < ||e_{j-1}||$ is to guarantee $||k_j(S_jL_{2,j} + S_jL_{1,j}S_{j-1}^{-1})|| < 1$. However, this sufficient condition (constraint) can be extremely demanding which can result in no solutions for the optimization problem in Eq. (8).

Learning Filter Design and Convergence Analysis. Rather than solving the optimization problem in Eq. (8), this section first presents a simple learning filter design as

$$L_{1,j} = 1 L_{2,j} = -S_{i-1}^{-1}$$
 (9)

that is, we keep $L_{1,j}$ fixed and vary $L_{2,j}$ iteratively. Design D_j as

$$D_i = c_d \hat{P}_i^{-1} Q_d \tag{10}$$

where c_d ($0 < c_d < 1$) is a weighting scalar to lower the sensitivity of the DOB, and Q_d is a low-pass filter to reduce the noise. Define

$$e_0 = T_i\{w\} = (P_i D_i \hat{P}_i - P_i)\{w\}$$
 (11)

as the measurement error recorded with the first agent which means there is no learning signal applied.

Next the learning convergence is analyzed. The heterogeneous agents have different system dynamics, that is, $S_j \neq S_{j-1}$ and $T_j \neq T_{j-1}$. With Eq. (10), we have

$$D_i \hat{P}_i = D_{i-1} \hat{P}_{i-1} \tag{12}$$

Then we have $P_j = \hat{P}_j(1+\Delta)$ in which Δ is bounded stable unknown dynamics to capture the modeling mismatch between the actual model and nominal model. Since this brief does not explicitly investigate modeling uncertainties, we reasonably assume Δ is small and for derivation purposes, it is rational to treat

$$P_j = \hat{P}_j \tag{13}$$

Though we did not quantify the modeling uncertainties, the model mismatch is not ignored and is explicitly considered in the numerical studies to show that the proposed method has some robustness to the modeling uncertainties, that is, different model mismatch is

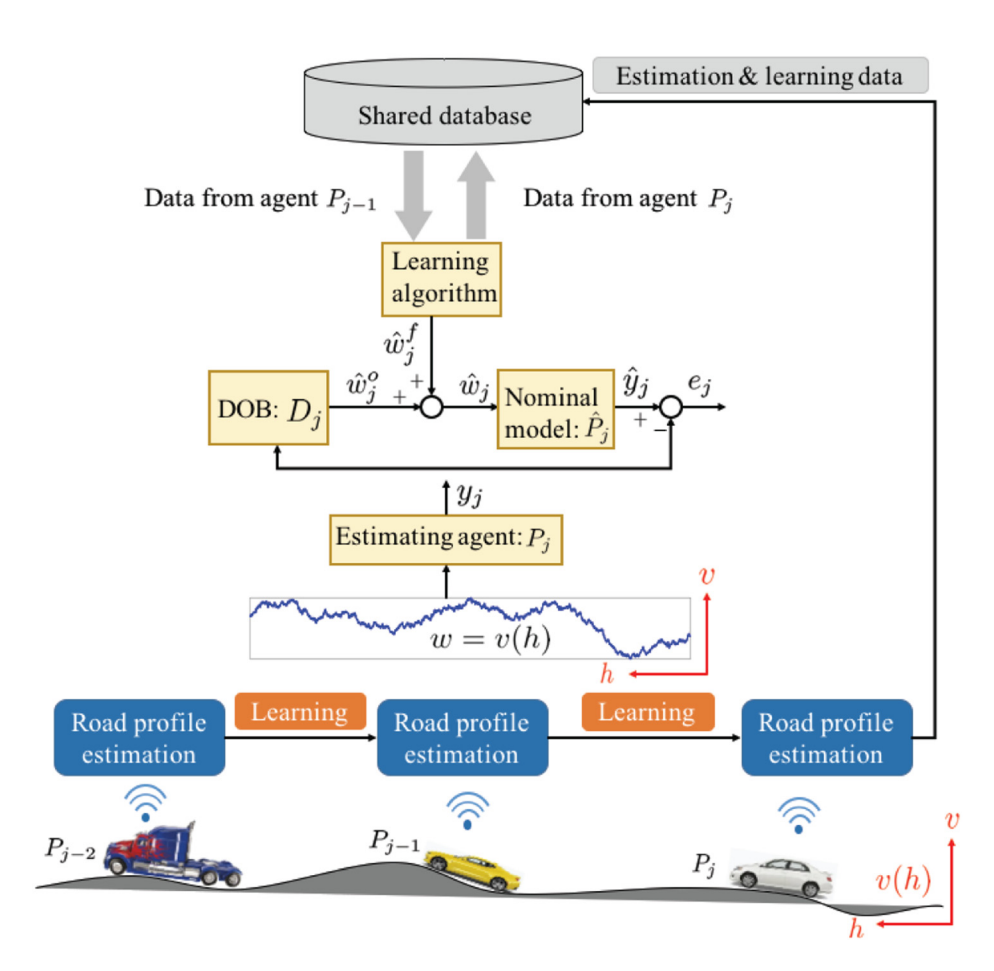


Fig. 3 Cascaded learning framework: agent j learns from agent j-1 for estimation enhancement

added to each different vehicle to simulate the practical scenarios. Then with Eqs. (1), (12), and (13), we have

$$T_{j}T_{j-1}^{-1} = P_{j}(D_{j}\hat{P}_{j} - 1)(D_{j-1}\hat{P}_{j-1} - 1)^{-1}P_{j-1}^{-1} = P_{j}P_{j-1}^{-1}$$
 (14)

and with Eqs. (1), (12), (13), and (14), we have

$$T_{j} - k_{j}S_{j}L_{1,j}S_{j-1}^{-1}T_{j-1}$$

$$= P_{j}P_{j-1}^{-1}T_{j-1} - k_{j}\hat{P}_{j}L_{1,j}\hat{P}_{j-1}^{-1}T_{j-1}$$

$$= (P_{j} - k_{j}\hat{P}_{j}L_{1,j}\hat{P}_{j-1}^{-1}P_{j-1})(D_{j-1}\hat{P}_{j-1} - 1)$$

$$= P_{j}(1 - k_{j}L_{1,j})(D_{j}\hat{P}_{j} - 1)$$
(15)

Plug Eqs. (9) and (15) into Eq. (7), and we have

$$e_{j} = (T_{j} - k_{j}S_{j}L_{1,j}S_{j-1}^{-1}T_{j-1})\{w\}$$

$$= (1 - k_{j})(P_{j}D_{j}\hat{P}_{j} - P_{j})\{w\}$$

$$= (1 - k_{j})\{e_{0}\}$$

$$= e_{j-1} - \eta e_{0}$$
(16)

Equation (16) indicates that the design with Eqs. (3), (4), and (9) guarantees the learning convergence since $k_j \le 1$. During this learning process, variable j can also be treated as the iteration index, and Eq. (16) implies that for the first several iterations while $k_j < 1$, the error e_j is reduced equally by ηe_0 in each learning iteration since η in Eq. (4) is a constant. The convergence rate of e_i depends on the design of k_i . For example, k_i can be set to be a quadratic or exponential function of the variable j, and based on Eq. (16), the convergence rate of e_i would be different. It is worth mentioning that the learning filters can be noncausal systems since the learning signals are generated offline, and this avoids introducing more delays in the learning signals; D_i is expected to have a basic estimation and therefore, extensive parameter design efforts for D_i are not needed. The inaccuracy from those basic estimations with D_i will be reduced through the learning iterations, and thus, the proposed learning method provides large design flexibility for D_i .

Numerical Validation

In this section, 20 heterogeneous agents are involved in the learning framework. A quarter-car dynamical model is used to generate the heterogeneous agents, while sinusoidal and type-C road profiles are used for estimation.

Quarter-Car Dynamical Model. A quarter-car model can be used to illustrate the road–vehicle interaction dynamics [14,22], as given in Fig. 4, where M_s and M_{us} denote the sprung mass (vehicle body) and the unsprung mass (vehicle wheel), respectively; k_s and k_{us} denote the spring stiffness, and c_s and c_{us} denote the damping coefficients. The vehicle suspension is modeled as a

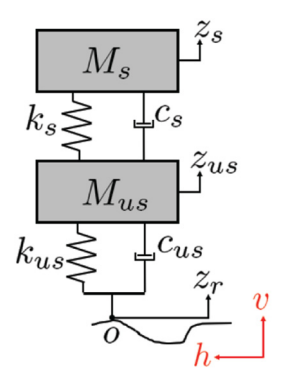


Fig. 4 Quarter-car dynamic model

Table 1 Dynamic parameter settings for the 20 agents (P_j) : the parameter value of each agent is a function of the agent index variable j; for each agent, model mismatch is introduced by generating a corresponding nominal model.

Parameter	Actual model P_j	Nominal model \hat{P}_j
M_s (kg)	2.45 + 0.1j	$(2.45 + 0.1j)f_m$
M_{us} (kg)	1 + 0.1j	1 + 0.1j
k_s (N/m)	950 + 10j	950 + 10j
k_{us} (N/m)	1250 + 10j	1250 + 10j
c_s (N s/m)	7.5 + 0.1j	7.5 + 0.1j
c_{us} (N s/m)	5 + 0.1j	5 + 0.1j

spring–damper system with k_s as its spring stiffness and c_s as its damping coefficient; the tire is modeled as another spring–damper system with k_{us} as its spring stiffness and c_{us} as its damping coefficient. z_r denotes the vertical displacement of the contact point c_p between the wheel and the road, and therefore z_r can be equally treated as the road profile; z_{us} and z_s denote the vertical displacements of M_{us} and M_s from their equilibrium points, respectively. When the vehicle travels through the road profile z_r , the system states z_{us} and z_s and their derivatives can be collected through sensors or estimation. The dynamic model from the road profile z_r to the displacement deflection z_s – z_{us} can be represented in the state-space form which can be referred to Ref. [14].

To generate 20 heterogeneous agents, we set different values for the dynamic parameters M_s , M_{us} , k_s , k_{us} , c_s , c_{us} shown in Fig. 4, and each set of those dynamic parameters will generate a linear time-invariant (LTI) system to represent agent P_i (j = 1, 2, ..., 20). The dynamic parameter values for each agent are given in Table 1, where j is the agent index number. For an individual agent, the value of the dynamic parameters all changes when a different j index is used. This is natural in practice since the road vehicles can have different values for each of the dynamic parameters. Also, for each agent P_j , a nominal model \ddot{P}_j is generated, where f_m is a scalar which will be assigned a random value within the range [0.96, 1.04] to add the model mismatch between P_i and \hat{P}_i . The model mismatch within each agent could be different since the f_m value is randomly generated. We can also introduce model mismatch by varying all the dynamic parameters instead of just varying M_s , but consider that model mismatch can come from several factors, including but not limited to the mass of the vehicle due to different numbers of passengers, the stiffness and damping coefficient of different tires, as well as modeling uncertainties from the nonlinearity, we choose to vary the vehicle mass as it is the most common and frequently changed parameter

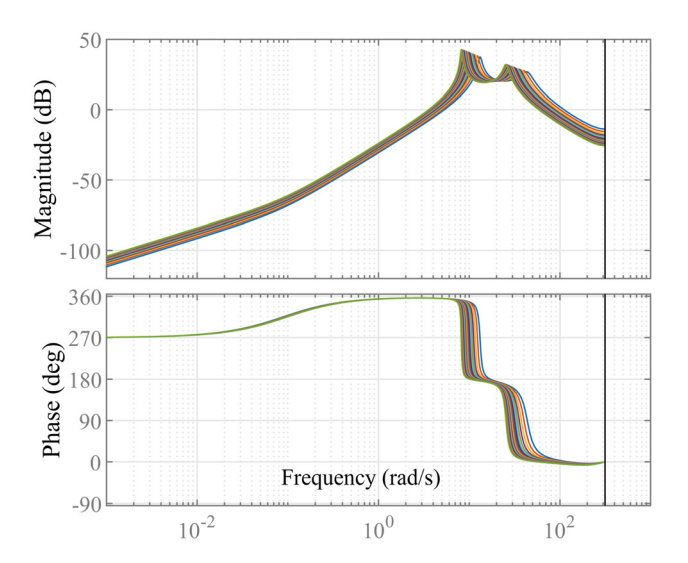


Fig. 5 Bode plots of the dynamics of 20 actual models

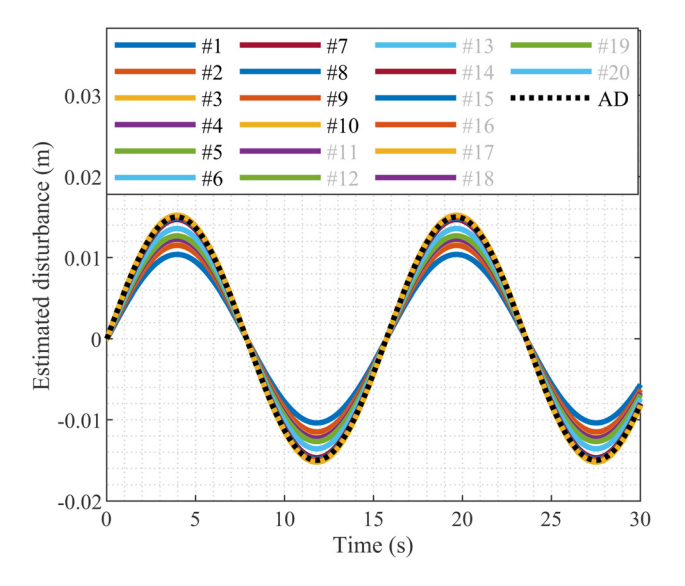


Fig. 6 Scenario 1: estimated disturbance (estimates from agent #11 to agent #20 are similar to that of agent #10, and are hidden for clear visual purposes)

for a vehicle. The bode plots of the dynamics of the 20 agents (\hat{P}_j) are given in Fig. 5, and each Bode plot represents a transfer function, which is generated by using the dynamic parameter values in Table 1, and the method to generate those transfer functions can be referred to Ref. [14]. Figure 5 shows that the dynamic difference among different agents lies in a wide frequency range, and satisfactory disturbance estimation is challenging to obtain with traditional DOB, which uses low-pass or bandpass filters to deal with uncertainties. This also motivates us to consider the proposed cascaded learning framework to enhance the estimation.

Estimation Scenarios. Estimation with the sinusoidal road profile input is defined as scenario 1, and the one with a type-C road profile is defined as scenario 2. The parameter c_d of all the DOBs is set to be 0.7, and the η is set as a constant value 1/7. The numerical studies of the two scenarios are as follows:

Scenario 1: The 20 agents travel through the same sinusoidal road profile as shown in the black dashed line labeled as "AD" in Fig. 6. The learning signal for each agent is provided in Fig. 7, where there is no learning signal for the initial learning iteration (agent #1). With the learning signals added to each corresponding agent's estimating loop, the disturbance estimation from each agent is given in Fig. 6. The estimation from agent #11 to #20 is not shown for clear visual purposes since those curves are similar to that of agent #10 and they are overlapped. The disturbance estimation error and its 2-norm are given in Figs. 8 and 9. Note that Fig. 9 indicates that the estimation from a latter agent (agent j) is closer to the actual road profile than its previous agent (agent j-1) until the error eventually converges. The 2-norm of the disturbance estimation error decreases for the first eight iterations, and the error is reduced by a near fixed amount for each estimation in the sense of 2-norm, which is consistent with Eq. (16). If we roughly connect the first eight dots in a line, we can treat that the 2-norm of the error decreases near linearly, and we refer it as a linear convergence. A different η would have led to a different line slope in Fig. 9. Therefore, the value η just changes the line slope (error convergence transient) but will not affect the steadystate error. By setting k_i as different functions (e.g., quadratic function of the index variable j), based on Eq. (16), the convergence rate of the 2-norm would be different and relative study results are omitted due to page limit. The 2-norm of the error varies and is bounded eventually, and this small variations are caused by the random model mismatch within each agent (the difference between P_i and its corresponding \hat{P}_i). The error would

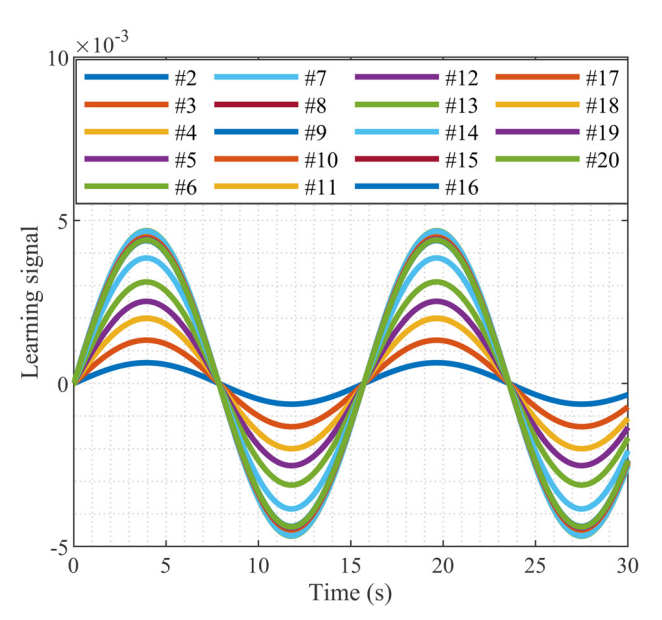


Fig. 7 Scenario 1: learning signal

converge smoothly to a constant value if this model mismatch is removed, as shown in Fig. 10. Figure 7 shows that the learning signal's magnitude also gradually increases and remains within a bounded region as to handle this random model mismatch.

Scenario 2: The same 20 agents travel through a type-C road profile, as given in the black dashed line labeled as AD in Fig. 11. This type-C road profile contains noisy and rough corners compared to the smooth sinusoidal profile used in scenario 1. The estimated disturbance from each agent is also given is Fig. 11; similarly, the estimation with agent #11 to agent #20 is not shown. The disturbance estimation error and its 2-norm with each agent are given in Figs. 12 and 13, and the learning signal for each agent is provided in Fig. 14. The results show that with the learning scheme, the disturbance estimation error is reduced over the learning iterations. To further show the effectiveness of the proposed learning framework, the estimation using only the same standard DOB without adding the learning signal to each agent is also carried out. The disturbance estimation is given in Fig. 15. The 2-norm of the estimation error is given in Fig. 16, and this

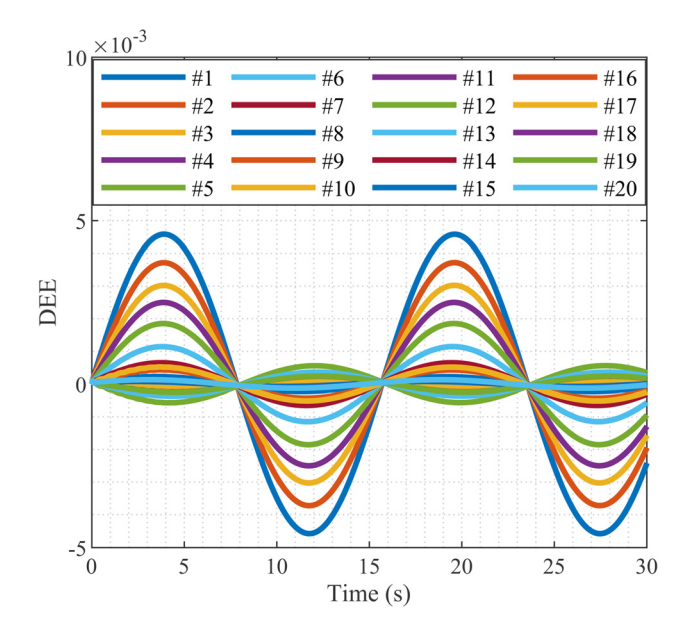


Fig. 8 Scenario 1: disturbance estimation error

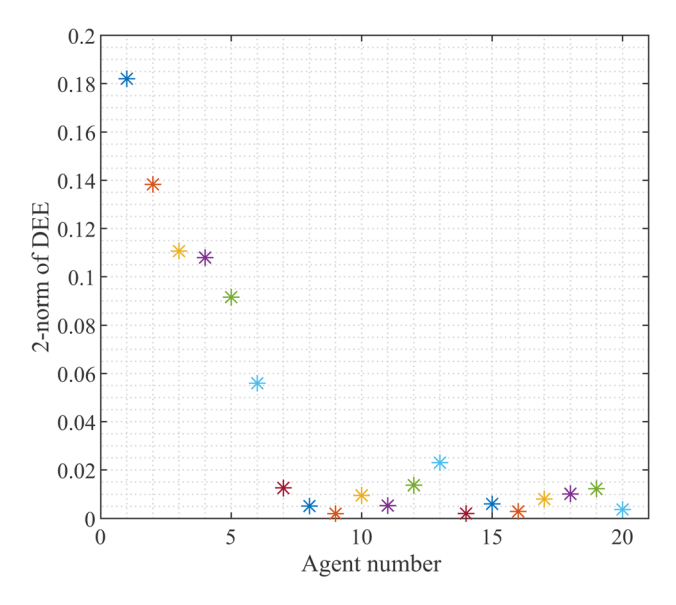


Fig. 9 Scenario 1: 2-norm of disturbance estimation error

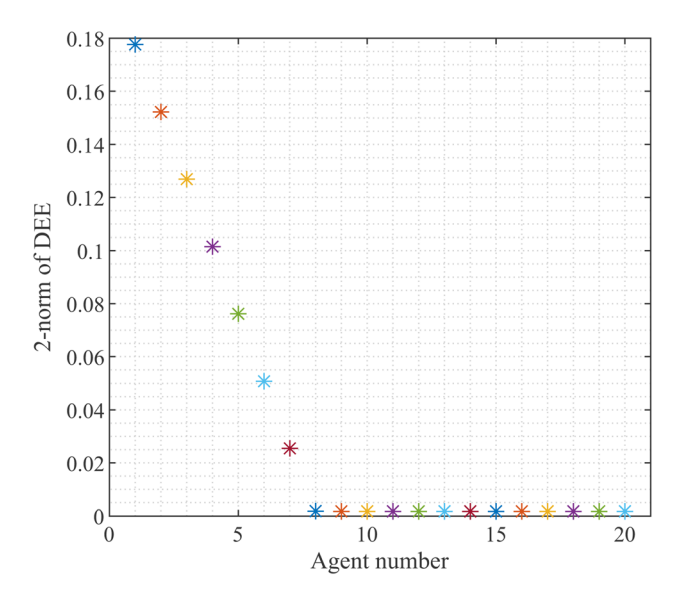
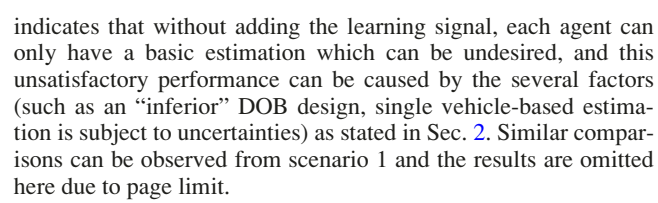


Fig. 10 Scenario 1: 2-norm of the disturbance estimation error (the model mismatch is removed)



To provide some insights statistically, we analyze the reduction of the estimation error in the sense of 2-norm for each scenarios: in Fig. 9, the initial error is 0.182, and the error with agent #10 is 0.009; in Fig. 13, the initial error is 1.846, and the error with agent #10 is 0.192. It is clear to see that the proposed method has reduced the error to a large extend for both scenarios. Note that the time steps in scenario 2 are larger than that in scenario 1, and this could result in a larger initial estimation error in the sense of 2-norm. And since the parameter k_j in Eq. (4) is designed as the same for the 2 scenarios, the convergence pattern would be similar. Though the modeling uncertainty is not quantified, the results show that the learning is effective with model mismatch presented. The advantages of the proposed method over the other

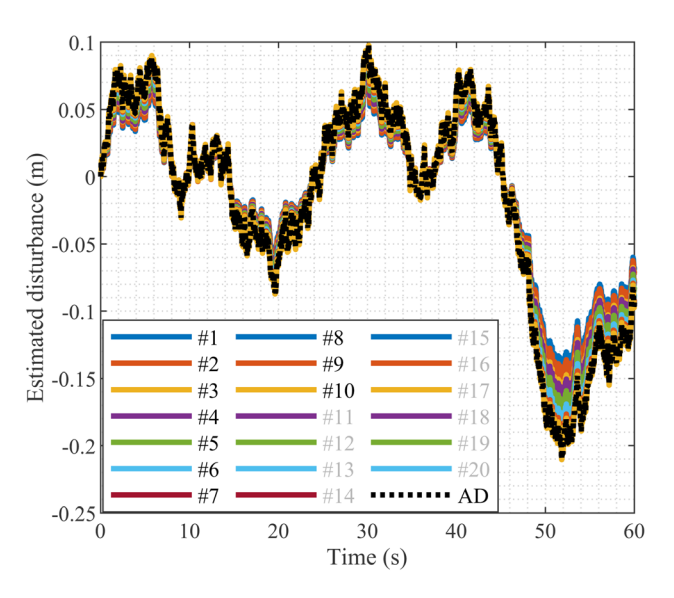


Fig. 11 Scenario 2: estimated disturbance; the initial estimate with agent #1 is not close to the actual disturbance, as can be seen in the area around 50 s

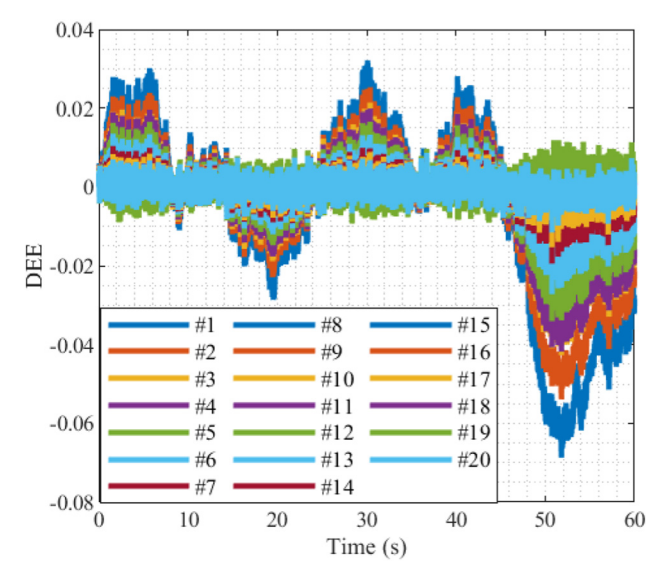


Fig. 12 Scenario 2: disturbance estimation error

single vehicle-based methods are that the proposed one does not need to design an accurate DOB or include a sophisticated feedback controller. Instead a basic DOB design is enough to have satisfactory performance by leveraging multiple vehicles. Moreover, the proposed method does not particularly aim to compete with other DOBs, but to provide a collaborative estimating method to (1) reduce the design efforts which can be demanding in other DOB designs; and (2) make the estimation less susceptible to uncertainties.

Conclusions

Concerning the road profile estimation scenario and improving from the single vehicle-based estimation, a cascaded learning framework was designed to achieve satisfactory performance by utilizing multiple heterogeneous vehicles. Through the learning mechanism, the estimation was iteratively pushed toward the actual one. A simple learning algorithm was presented and the learning convergence was analyzed. Sinusoidal and type-C road profiles were tested in the numerical studies to validate the effectiveness of the proposed method. In our future work, we plan to

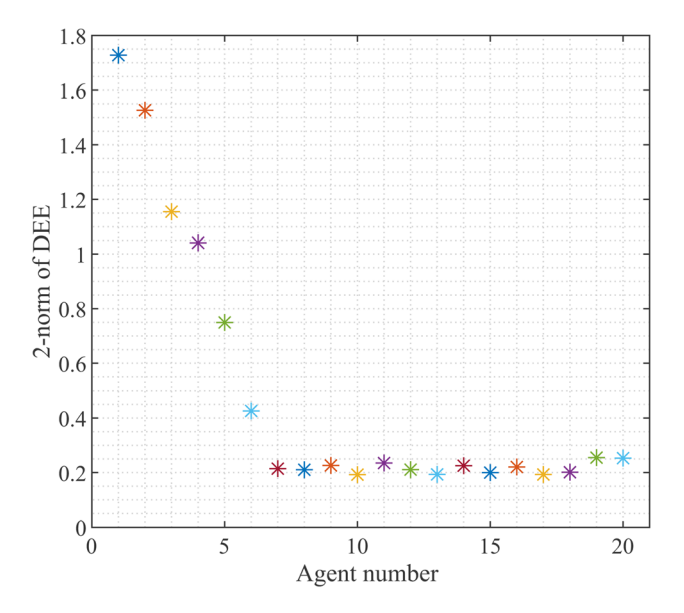


Fig. 13 Scenario 2: 2-norm of the disturbance estimation error

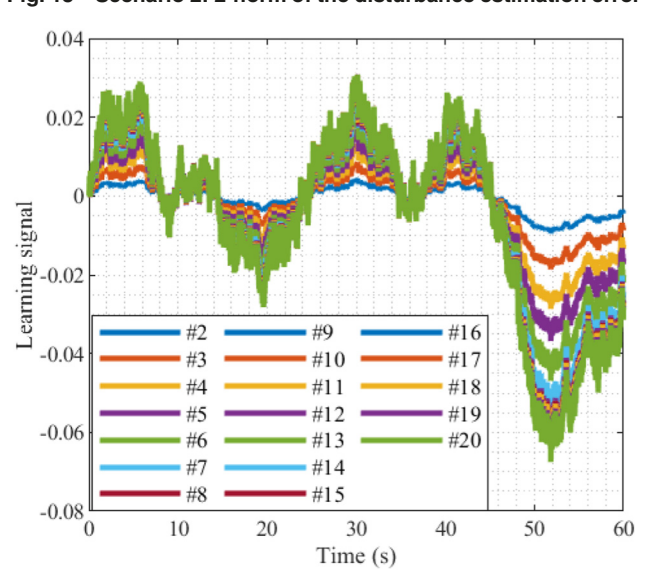


Fig. 14 Scenario 2: learning signal

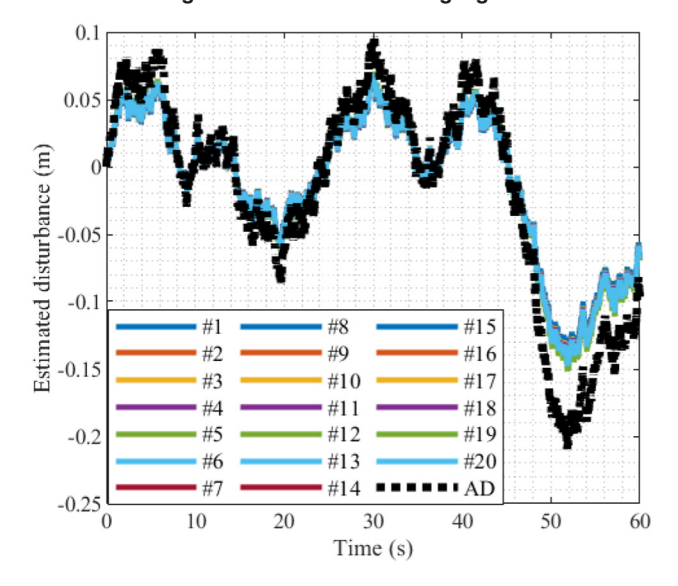


Fig. 15 Scenario 2: disturbance estimation when no learning signal is added to the agents

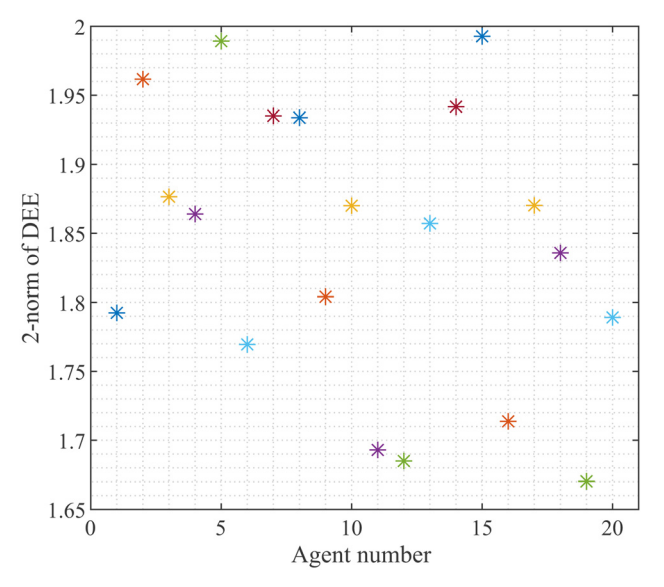


Fig. 16 Scenario 2: 2-norm of the disturbance estimation error when no learning signal is added to the agents

explicitly analyze the proposed method's robustness to modeling uncertainties, and validate the method exhaustively via experimental tests.

Acknowledgment

This material is based upon work supported by the National Science Foundation—the USA under Grants No. 2030411/2030375. Any opinions, findings, and conclusions, or recommendations expressed in this material are those of the authors and do not necessarily reflect the views of the National Science Foundation.

Funding Data

 Directorate for Engineering (Grant Nos. 2030375 and 2030411; Funder ID: 10.13039/100000084).

References

- Li, Z., Kolmanovsky, I., Atkins, E., Lu, J., Filev, D., and Michelini, J., 2014, "Cloud Aided Semi-Active Suspension Control," IEEE Symposium on Computational Intelligence in Vehicles and Transportation Systems (CIVTS), Orlando, FL, Dec. 9–12, pp. 76–83.
- [2] Li, Z., Kolmanovsky, I. V., Atkins, E. M., Lu, J., Filev, D. P., and Bai, Y., 2017, "Road Disturbance Estimation and Cloud-Aided Comfort-Based Route Planning," IEEE Trans. Cybern., 47(11), pp. 3879–3891.
- [3] Healey, A., Nathman, E., and Smith, C., 1977, "An Analytical and Experimental Study of Automobile Dynamics With Random Roadway Inputs," ASME J. Dyn. Syst., Meas., Control, 99(4), pp. 284–292.
- [4] Doumiati, M., Victorino, A., Charara, A., and Lechner, D., 2011, "Estimation of Road Profile for Vehicle Dynamics Motion: Experimental Validation," Proceedings of the American Control Conference, San Francisco, CA, June 29–July 1, pp. 5237–5242.
- [5] McCann, R., and Nguyen, S., 2007, "System Identification for a Model-Based Observer of a Road Roughness Profiler," IEEE Region 5 Technical Conference, Fayetteville, AR, Apr. 20–21, pp. 336–343.
- [6] Ni, T., Li, W., Zhao, D., and Kong, Z., 2020, "Road Profile Estimation Using a 3D Sensor and Intelligent Vehicle," Sensors, 20(13), p. 3676.
 [7] Xue, K., Nagayama, T., and Zhao, B., 2020, "Road Profile Estimation and Half-
- [7] Xue, K., Nagayama, T., and Zhao, B., 2020, "Road Profile Estimation and Half-Car Model Identification Through the Automated Processing of Smartphone Data," Mech. Syst. Signal Process., 142, p. 106722.
- [8] Moghadam, A., and Sarlo, R., 2021, "Application of Smartphones in Pavement Profile Estimation Using Sdof Model-Based Noisy Deconvolution," Adv. Civ. Eng., 2021, pp. 1–13.
- [9] Whaiduzzaman, M., Sookhak, M., Gani, A., and Buyya, R., 2014, "A Survey on Vehicular Cloud Computing," J. Network Comput. Appl., 40, pp. 325–344.
- [10] Zhao, W., Zhang, H., and Li, Y., 2018, "Displacement and Force Coupling Control Design for Automotive Active Front Steering System," Mech. Syst. Signal Process., 106, pp. 76–93.
- [11] Rath, J., Veluvolu, K. C., and Defoort, M., 2014, "Estimation of Road Profile for Suspension Systems Using Adaptive Super-Twisting Observer," European Control Conference (ECC), Strasbourg, France, June 24–27, pp. 1675–1680.

- [12] Zheng, M., Chen, X., and Tomizuka, M., 2016, "Extended State Observer With Phase Compensation to Estimate and Suppress High-Frequency Disturbances, American Control Conference (ACC), Boston, MA, July 6–8, pp. 3521–3526.
- [13] Lyu, X., Zheng, M., and Zhang, F., 2018, "Hinfinity Based Disturbance Observer Design for Non-Minimum Phase Systems With Application to Uav Attitude Control," Annual American Control Conference (ACC), Milwaukee, June 27-29, pp. 3683-3689.
- [14] Li, Z., Zheng, M., and Zhang, H., 2019, "Optimization-Based Unknown Input Observer for Road Profile Estimation With Experimental Validation on a Suspension Station," American Control Conference (ACC), Philadelphia, PA. July 10–12, pp. 3829–3834.
- [15] Hassen, D. B., Miladi, M., Abbes, M. S., Baslamisli, S. C., Chaari, F., and Haddar, M., 2019, "Road Profile Estimation Using the Dynamic Responses of the Full Vehicle Model," Appl. Acoust., 147, pp. 87–99.
 [16] Hamersma, H. A., and Els, P. S., 2021, "Vehicle Suspension Force and Road
- Profile Prediction on Undulating Roads," Veh. Syst. Dyn., 59(10), pp.
- [17] Tudón-Martínez, J. C., Fergani, S., Varrier, S., Sename, O., Dugard, L., Morales-Menendez, R., and Ramírez-Mendoza, R., 2013, "Road Adaptive Semi-Active Suspension in an Automotive Vehicle Using an LPV Controller,' IFAC Proc. Vol., 46(21), pp. 231–236.
- [18] Pusadkar, U. S., Chaudhari, S. D., Shendge, P., and Phadke, S., 2019, "Linear Disturbance Observer Based Sliding Mode Control for Active Suspension Systems With Non-Ideal Actuator," J. Sound Vib., 442, pp. 428-444.
- [19] Ngwangwa, H. M., Heyns, P. S., Breytenbach, H. G. A., and Els, P. S., 2014, "Reconstruction of Road Defects and Road Roughness Classification Using

- Artificial Neural Networks Simulation and Vehicle Dynamic Responses: Application to Experimental Data," J. Terramech., 53, pp. 1-18.
- [20] Qin, Y., Langari, R., Wang, Z., Xiang, C., and Dong, M., 2017, "Road Excitation Classification for Semi-Active Suspension System With Deep Neural Networks," J. Intell. Fuzzy Syst., 33(3), pp. 1907–1918.

 [21] Cronin, L. M., Eshkevari, S. S., Sen, D., and Pakzad, S. N., 2021, "Transfer Learning for Input Estimation of Vehicle Systems," IEEE International Confer-
- ence on Acoustics, Speech and Signal Processing (ICASSP), Ontario, ON, Canada, June 6-11, pp. 7953-7957.
- [22] Gao, H., Li, Z., and Wang, Y., 2020, "Privacy-Preserved Collaborative Estimation for Networked Vehicles With Application to Road Anomaly Detection," arXiv:2008.02928.
- [23] Zheng, M., Lyu, X., Liang, X., and Zhang, F., 2020, "A Generalized Design Method for Learning-Based Disturbance Observer," IEEE/ASME Trans. Mechatronics, 26(1), pp. 45-54.
- [24] Song, S., and Wang, J., 2020, "Incremental Model Predictive Control of Active Suspensions With Estimated Road Preview Information From a Lead Vehicle," ASME J. Dyn. Syst., Meas., Control, 142(12), p. 121004.
- [25] Chen, Z., Liang, X., and Zheng, M., 2020, "Knowledge Transfer Between Different Uavs for Trajectory Tracking," IEEE Rob. Autom. Lett., 5(3), pp. 4939-4946.
- [26] Chen, Z., Liang, X., and Zheng, M., 2022, "Iterative Learning for Heterogeneous Systems," IEEE/ASME Trans. Mechatronics, 27(3), pp. 1510-1521.
- [27] Liu, N., and Alleyne, A., 2016, "Iterative Learning Identification for Linear Time-Varying Systems," IEEE Trans. Control Syst. Technol., 24(1), pp. 310-317.